applied sciences

MDPI

Article

High-Performance Solid Medium Thermal Energy Storage System for Heat Supply in Battery Electric Vehicles: Proof of Concept and Experimental Testing

Volker Dreißigacker * and Lukas Hofer

Institute of Engineering Thermodynamics, German Aerospace Center, Pfaffenwaldring 38-40, 70569 Stuttgart, Germany
* Correspondence: volker.dreissigacker@dlr.de; Tel.: +49-711-6862-449

Abstract: The reduction of global CO_2 emissions requires cross-sectoral measures to reduce fossil energy consumptions and to strengthen the expansion of renewable energy sources. One element for this purpose are thermal energy storage systems. They enable, due to their time-decoupled operation, increases in systemic efficiency and flexibility in various industrial and power plant processes. In the electricity and heat sector such solutions are already commercially available for large-scale applications or are focused in diverse R&D projects, but are largely new in the transport sector. By transferring existing concepts specifically to the requirements for the heat supply of battery electric vehicles, efficiency improvements can also be achieved in the transport sector. The idea is to provide the required heat for the interior during cold seasons via a previously electrical heated thermal energy storage system. Thus, battery capacities can be saved, and the effective range of the vehicle can be increased. Basic prerequisites for this concept are high systemic storage densities and high performances, which must be justified to commercial battery powered PTC-elements. Compared to large-scale applications, this results in new challenges and design solutions needing finally a proof of concept and experimental tests under vehicle typical specifications. For the first time, a novel thermal energy storage system based on ceramic honeycombs with integrated heating wires and a double-walled, thermally insulated storage containment was developed and constructively realized. This storage system meets all the requirements for the heat supply, reaches high systemic storage and power densities and allows due to its high flexibility a bifunctional operation use: a cyclic storage and a conventional heating mode. In the focused storage operation, high-temperature heat is generated electrically through heating wires during the charging period and transferred efficiently via thermal radiation to the ceramic honeycombs. During the discharging period (driving) the stored thermal energy is used for heating the interior by a bypass control system at defined temperatures with high thermal output. The systematic measurement campaigns and successful model validations confirm high electrical heating powers of 6.8 kW during the charging period and a heat supply with a thermal output of 5 kW over more than 30 min during the discharging period. Despite current infrastructure and test rig restrictions, high systemic storage densities of 155 Wh/kg with constant discharging outlet temperatures are reached. Compared to battery powered heating systems, the experimental results for the developed thermal energy storage system confirm an excellent level of competitiveness due to its high performance, operational flexibility and low-cost materials.

Keywords: solid medium thermal energy storage system; battery electric vehicles; proof of concept

Citation: Dreißigacker, V.; Hofer, L. High-Performance Solid Medium Thermal Energy Storage System for Heat Supply in Battery Electric Vehicles: Proof of Concept and Experimental Testing. *Appl. Sci.* **2022**, *12*, 10943. https://doi.org/10.3390/app122110943

Academic Editor: Luisa F. Cabeza

Received: 5 September 2022
Accepted: 26 October 2022
Published: 28 October 2022

1. Introduction

Worldwide CO_2 emissions and the associated global warming are forcing the exit of fossil-fueled processes in industrial applications, in electricity and heat production as well as in the transport sector. In particular for the ground-based transport sector, significant CO_2 reduction can be expected as a result of increasing number of battery electric vehicles

(BEV) together with renewable energies. Further efficiency improvements for those vehicles are needed to increase acceptance in terms of effective range.

In addition to technological advances in battery development, new thermal management concepts play a central role, allowing electrical energy consumption for cabin climatization to be minimized. For example, current battery-powered PTC heaters lead to range losses of up to 50% during cold seasons [1,2], whereas efficient heat pump systems with lower electrical energy demands allow effective range improvements. Another promising technology are thermal energy storage systems. They improve as a separate component or in combination with heat pumps the overall efficiency, thus range extensions.

So far, commercial as well as R&D based activities focus on large scale applications, e.g., for the flexibilization of industrial [3,4] or power plant processes [5,6] as well as for novel electrical heated storage systems [7,8]. The basic idea is to store heat efficiently in the process at times of low thermal energy demand (charging period) and to provide it to the process at times of increased thermal energy demand (discharging period). With this time-decoupled operation systemic efficiency and flexibility improvements are achieved.

Thermal energy storage systems are classified as sensible [9,10], latent [11] or thermochemical systems [12], whereby their application potential depends on the maximum operating temperature, the heat transfer medium, the charging/discharging durations or system requirements. Additionally, technological developments have been taking place for some years towards upscaled high-temperature heating systems. These concepts allow in combination with thermal energy storage systems additional increases in systemic flexibility and cost efficiency. Particularly for sensible thermal energy storage systems based on solids, inductive or conductive heating systems are being developed, which aim to elevate the temperature level with simultaneous high load gradients [13].

Compared to large-scale applications, studies on the application potential of thermal energy storage systems in the transport sector have so far played a minor role. Except for preheating of catalysts [14] and combustion engines [15] as well as for cooling applications [16], investigations were mainly focused on thermochemical storage systems (gas-solid reactions), offering an alternative heat and cold supply [17,18] for fuel cell vehicles. In recent years, an increasing number of publications have appeared for the heat supply of battery electric vehicles with thermal energy storage concepts based on phase change materials (PCM) [19–22] and on solid media [23,24]. Here, during the charging period the required heat is generated electrically, transferred to the storage material and used during discharging for heating the interior by a mass flow-controlled bypass. For a successful use of such thermal energy storage concepts in battery electric vehicles, systemic benefits compared to conventional battery powered PTC systems must be given. This challenge is strongly linked with high systemic storage and power densities and must be justified on today's commercial Li-Ion batteries operating in a range from 110 Wh/kg to 160 Wh/kg [25].

A favorite technology for this purpose is based on electrically heated solid medium thermal energy storage system (regenerator), which achieves all target values in terms of high charging/discharging performance, constant discharge temperature and high systemic storage densities. Their high thermal efficiency is a result on a wide range of geometrical inventory options with high specific heat transfer surfaces, a direct contact between the solid and the fluid phase and powerful electrical resistance heating systems. Such a storage system with honeycomb-shaped ceramic solids was investigated in [26]. Under neglection of the containment mass, high systemic storage densities of up to 285 Wh/kg with constant electrical charging and thermal discharging powers of more than 5 kW were identified. Despite these successes, the findings presented so far are based only on simulative results. Experimental investigations are need to confirm the feasibility and performance.

Previous experimental works on such applications can be found for thermal storage systems based on phase change materials [27,28], whereby the investigations were focused on feasibility and systemic storage density under simplified requirements. However, for

a successful application of thermal storage systems, experimental investigations under vehicle-typical boundary conditions are necessary.

For the first time, experimental results are presented for a thermal energy storage system based on solids. This system meets all vehicle-specific requirements and reaches high systemic storage densities despite test rig-related limitations. In addition, the high operational flexibility of the novel component is tested allowing—aside the cyclic storage mode—a use as conventional PTC heating system. The results presented below and the optimization potential identified provide a significant contribution to increasing the efficiency of battery electric vehicles and thus their effective range.

2. Thermal Storage System

Key challenges in the development of thermal storage systems for the heat supply in battery electric vehicles are—in addition to cost efficiency—high systemic storage densities with simultaneously high performances. For both sensible and latent systems, this requires high temperatures in the storage medium as well as an effective heat transport during both the charging and discharging period. In particular, thermal energy storage systems based on solids open up very high potentials for achieving these desired goals due to their variety of geometries, high-temperature, cost-effective and durable materials.

The basic idea of such thermal batteries is to generate heat electrically (parallel of charging the battery), to transfer and store it efficiently in the storage medium and to provide it at a defined temperature level with high thermal power during the discharging period (driving) by using a bypass control system. For this purpose, extensive concept developments, detailed modeling and design calculations [24,26] have been performed, whose results formed the base for the realization and investigations presented here. A schematic representation of the favorite thermal storage concept including the central subsystems and heat transport processes is shown in Figure 1.

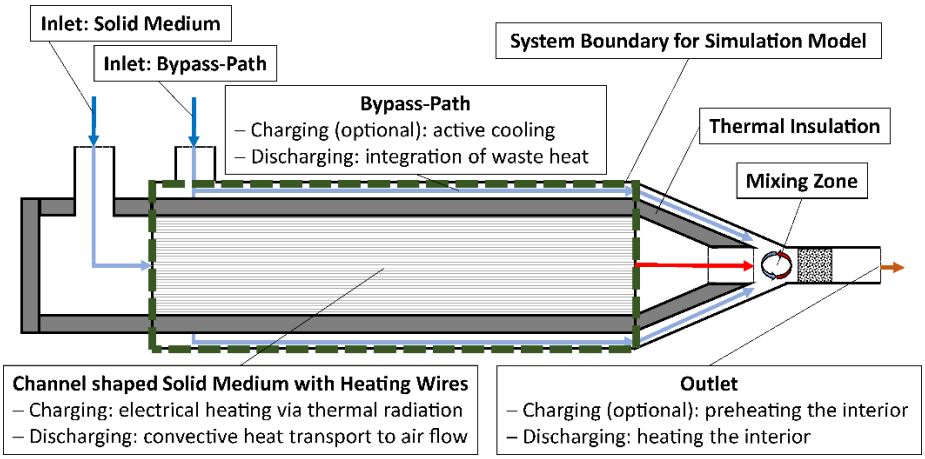

Figure 1. Schematic representation of the favorite thermal storage concept [24,26].

The electrical heating of the storage system (charging period) is based on heating wires, which are homogeneously integrated within the channel-shaped inventory structure enabling large-area and powerful heating of the electrically non-conductive ceramic storage material (here: Al_2O_3) via thermal radiation. During the thermal discharge operation, the (cold) ambient air passes mass flow controlled the bypass and the channel-shaped inventory path in order to achieve constant mixing temperatures at a at the outlet of the storage system. Inside the inventory path, the previously electrical generated and stored high temperature heat is transferred convectively form the solid to the fluid flow. For efficiency improvements, the bypass path encloses the thermal insulation on the shell side to integrate heat losses during discharging period convectively into the air flow. Due its integrated construction, the bypath path can be also used (optional) for preheating the interior through a slight active cooling of the thermal insulation during charging period.

The modeling of the presented storage concept was based on radially coupled subsystems for the channel shaped inventory structure, the thermal insulation and the bypass path. For calculation of temporal and local temperatures, 2D-based models were used for the storage inventory and the thermal insulation, and a 1D-based model was used for the bypass patch. Specifically, for the channel shaped storage inventory, a heterogeneous porous approach was used that distinguishes between fluid and solid phases and captures convective and conductive heat transfer resistances. The heat balance equation for the solid phase was extended by a homogeneously distributed source term with respect to the integrated heating wires, which heats the storage inventory during charging period via thermal radiation. In order to limit the heating power to a maximum permitted heating wire temperature, a power control was implemented. Additionally, a further control algorithm was integrated to enable constant mixing temperatures during thermal discharging at the outlet through an automatized distribution of the mass flow to the bypass and the storage inventory path.

The radial coupling of the subsystems is based on thermal contact resistance, convective heat transfer and thermal radiation. For the total storage system, temperature-averaged material data were applied as well as axial and radial boundary conditions: axially, adiabatic boundary conditions were assumed, radially, convective heat losses to the environment. The partial differential equations were discretized locally using central and backward difference methods, respectively, and the resulting differential algebraic equation system was solved in time via Matlab. Central input variables include during charging period the electrical heating power, the maximum permitted heating wire temperature and the optional active cooling mass flow rate in the bypass path and during discharging period the cold entering total mass flow rate as well as the constant mixing temperature to be achieved. Detailed information on modeling, the radiant heating system and the bypass path are described in [24,26].

3. Experimental Set-Up

Central elements of the thermal storage system test rig include the ceramic, channel shaped inventory (honeycomb) with integrated heating wires, the shell sided thermal insulation and the double-wall containment with integrated bypass. The test rig design was based on simulation studies on the storage system [24,26] reaching a constant thermal output of 5 kW over 30 min during the discharging period and is heated in less than 30 min during the charging period. Based on these simulative results, commercially available inventories, heating wire options and microporous thermal insulations, technical specifications for the overall design were developed and realized in exchange with suppliers. Central parameters for favorite design options and for the finally erected test rig with an electrical power supply of 400 V and a maximum current of 16 A are summarized in Table 1.

Table 1. Central specification for the favorite design solution: simulation results vs. test rig.

Subsystem		Simulation Results	Test Rig
Storage Inventory	Material	Al_2O_3	91% Al_2O_3
	Mass [kg]	8.2	2 × 5.9
	Specific Surface [m^2/m^3]	>200	620
	Void Fraction [%]	40–70	66
	Length-to-Diameter Ratio	2–4	3.65
Heating Wire	Material	FeCrAl Alloy	FeCrAl Alloy
	Maximum Operation Temperature [°C]	1000	1300
	Length [m]	30	3 × 30
	Diameter [mm]	1.5	1.5
Thermal Insulation	Typ	microporous	microporous
	Thickness [mm]	20–40	25

The storage inventory selected here (honeycomb) with an Al_2O_3 content of 91% shows high specific surface areas of 620 m^2/m^3 at void fractions of 66% and exceeds significantly the required geometric specifications in terms of heat transferring surface compared to the simulation results from Table 1. Due to manufacturing constraints, two honeycombs were installed here behind each other, with a total mass of 11.8 kg, a length (L) of 566 mm with a diameter of 155 mm.

Inside the honeycombs three heating wires were integrated allowing operating temperatures of 1300 °C, whereby each has a diameter of 1.5 mm, a length of 30 m and were selected for maximum permitted currents of 16 A at a voltage of 400 V. In total, this results in a mass of 1.2 kg and a maximum heating power of 19.2 kW, which is significantly higher than the target values to be achieved. Unfortunately, the delta circuit required therefor using a 400 V three-phase alternating current could not be implemented due to laboratory restrictions, since the resulting maximum current in the outer conductor would exceed the permitted electric fuse of 16 A. Hence, the three heating wires were connected in a star circuit, which limited the maximum heating power in total to 6.8 kW. However, by adapting the laboratory infrastructure on a 32 A system and a delta circuit, heating powers of 19.2 kW can be achieved in the future. Central insights into the honeycombs with integrated heating wires are shown in Figure 2.

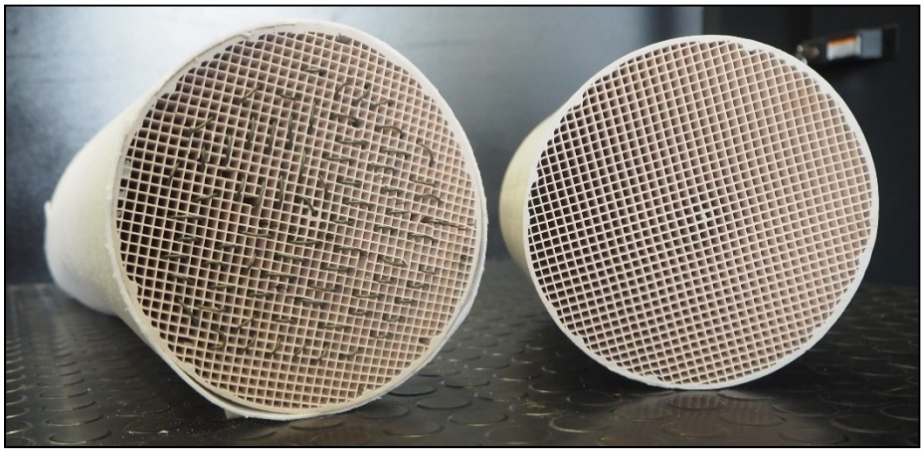

Figure 2. Ceramic honeycombs without (**right**) and with integrated heating wires (**left**)—dimensions: diameter of 155 mm with a total length of 566 mm.

The double-walled containment with integrated bypass including the air-side piping connections was made of aluminum with a wall thickness of 0.6 mm and reaches a total mass of 5.9 kg. The heating wires were integrated into the storage system through thermally decoupled electrode line bushings and additionally thermally insulated within the flow distribution chamber. Microporous thermal insulations with a layer thickness of 25 mm were installed inside the containment on the shell side and at the conical outlet of the storage inventory. For other zones still internally uninsulated (inlet and outlet areas), high-temperature fiber blankets were used, resulting in a mass of 2.5 kg for all thermal insulations. In total, the test rig reaches a mass of 21.4 kg without measuring devices and is shown in Figure 3.

Due to the high amount of measuring devices and the required accessibility therefor, the dimension of the double-walled storage containment was significantly oversized. Future work will focus on volume-specific optimization, among other things by reducing distribution volumes, heating wire lengths, containment design and measuring devices.

An overview of the central measuring points within the thermal storage system, in order to record all the variables required for validation and to identify optimization potentials, is shown schematically in Figure 4.

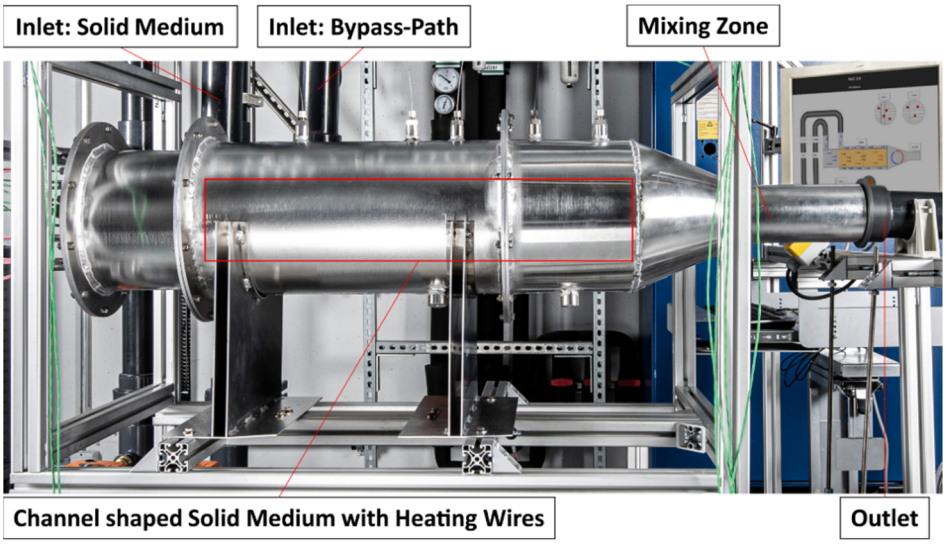

Figure 3. Test Rig—electrically heated thermal storage system based on solid materials.

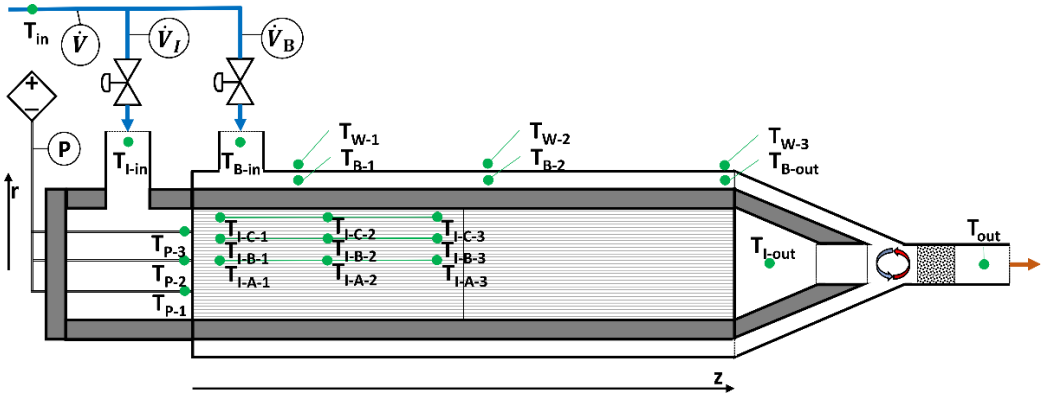

Figure 4. Central measuring points.

Within the storage system a total amount of 21 thermocouples (type K and type N) with an accuracy of ±1.5 °C or ±0.4% were integrated as well as one PT100 each at the inlet and outlet with an accuracy of ±0.15 °C or ±0.2%, allowing a complete detection of the transient (t) temperature profiles (T). Inside the storage inventory (I) three radially (r) distributed multipoint- thermocouples (A at r = 0 mm, B at r = 25 mm, C at r = 70 mm) were placed, each with three axial (z) measuring points. Here, due to accessibility only temperature measurements were feasible in the first honeycomb at z/L = 0.05, z/L = 0.25 and z/L = 0.45. In addition to the bypass path (subscript *B*), the shell-side outer surface (subscript *W*) and the three heating wires (subscript *P*), temperatures were recorded at entry (subscript *in*) and exit (subscript *out*) points.

The total volume flow rate of up to 200 Nm^3/h required to discharge the storage system was provided via the inhouse compressed air supply. Two membrane valves were used for volume flow-controlled regulation of the constant mixing temperature via the bypass and the inventory path to enable a reliable operation control with a high degree of accuracy. In addition to the single volume flow rates ($\dot{V}$), each with a measurement accuracy of 2%, the electrical power (P) was recorded via a multifunctional power meter with a measurement accuracy of 1%.

Based on the test rig presented here as well as the measuring devices, systematic and sequential measurement campaigns including model validation are presented in the following.

4. Results

The experimental investigations focus on systematic and sequential measurement campaigns regarding three central aspects of the thermal storage system: during charging period the active cooling within the double-wall containment and the electrical heating power as well as during discharging period the constant thermal output and discharge duration to be achieved. Extensive measurements were conducted on each of these aspects, which are exemplarily explained in detail at the beginning of each section, followed up by a summary of the central results. Additionally, simulation results are presented to allow statements on model quality or on missing model aspects. Here, simulation inputs are the given boundary conditions or target values, which are summarized for each measurement campaign at the beginning.

4.1. Charging Period: Active Cooling

The design of the storage system is based on a shell sided integration of the bypass path around the thermal insulation with the idea to utilize heat loss during discharging period and to enable preheating of the interior during charging period by a slight active cooling. To investigate these effects during charging period, a moderate thin thermal insulation with a thickness of 25 mm was chosen to achieve significant temperature changes in the bypass path.

For this purpose, steady-state series of measurements were performed that included variations of the bypass mass flow rate ($\dot{m}_B$) and the average inventory temperature ($\overline{T}_I$). In this case, the tTe storage system was heated at the beginning with an electrical heating power of 5 kW and kept stationary—after reaching the defined average inventory temperature—by the implemented power control. Central variation parameters are summarized in Table 2.

Table 2. Central variation parameters: average inventory temperature ($\overline{T}_I$) and bypass mass flow rate ($\dot{m}_B$).

$\overline{T}_I$ [°C]	$\dot{m}_B$ [kg/h]
365	14
555	40
755	65
835	89
	113

For two exemplary selected measurements at $\overline{T}_I$ = 835 °C and $\dot{m}_B$ = 14 kg/h as well as at $\overline{T}_I$ = 835 °C and $\dot{m}_B$ = 113 kg/h, the resulting steady-state temperatures at the outlet of the bypass path (T_{B-out}) are shown in Figure 5.

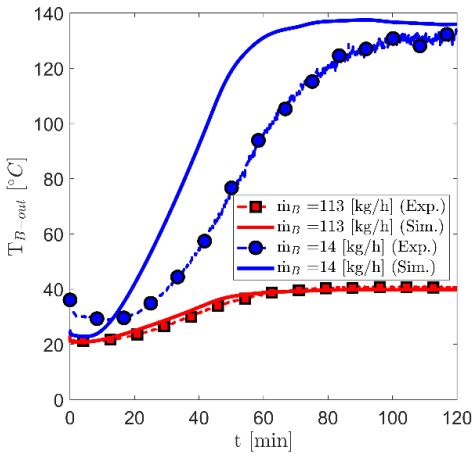

Figure 5. Transient characteristics of the bypass outlet temperature (T_{B-out}).

The results under steady state conditions show the well-known relationship of increasing mass flow rates with simultaneously decreasing outlet temperatures in both the measurement and simulation characteristics. Related to the experimental data, slightly higher steady-state active cooling powers of 570 W result here at a mass flow of 113 kg/h compared to 420 W at a mass flow of 14 kg/h. Similar orders of magnitude with 540 W and 440 W are also reached in the simulative results. These effects are caused by increasingly convective heat transfer coefficients associated with higher mass flow rates. In addition to comparable steady-state results, the transient characteristics between the experimental and simulative temperatures also show a good agreement. Larger deviations can be seen especially at low mass flow rates, which can be explained by the neglection of the thermal mass of the bypath channel inside the model.

Analogous to the exemplarily presented contexts, all results within the conducted measurement campaign for active cooling show comparably characteristics with good agreements between experiment and simulation. The resulting central steady-state results based on the investigations according to Table 2 are summarized in Figure 6.

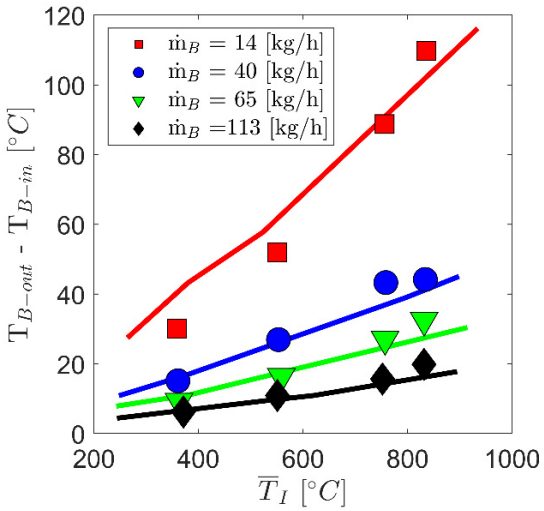

Figure 6. Steady-state bypass temperature differences between outlet (T_{B-out}) and inlet (T_{B-in}) as a function of average inventory temperatures ($\overline{T}_I$)—experimental results illustrated with symbols, simulative results with lines.

As can be seen, increasing steady-state temperature differences between the outlet and inlet bypass are associated with higher average inventory temperatures and decreasing active cooling mass flow rates. Furthermore, the simulation results also show comparable magnitudes and characteristics and thus confirm the quality of the implemented heat transport mechanisms within the model.

For further measurement campaigns presented in the following, the active cooling mass flow rate was activated after a maximum permitted temperature in the bypass path has been exceeded. The magnitude of the active cooling mass flow rate ($\dot{m}_{B,c}$) was selected in such a way, that a maximum bypass outlet temperature of 60 °C results under steady state condition. For this purpose, the results according to Figure 6 were used at a temperature difference of 40 °C, since the inlet temperatures within the measurement campaigns showed constant values of approx. 20 °C. The linear function of active cooling mass flow rate (in kg/h) depending on the average inventory temperature (in °C) were interpolated from this leading to:

$$\dot{m}_{B,c} = \min\left(0\ ,\ 0.095\ \overline{T}_I - 26.1\right) \tag{1}$$

The relation given in Equation (1) was implemented in both the measurement and simulation procedures. The results on time of activating the active cooling mass flow rate ($\dot{m}_{B,c}$) as well as on the transient heating of the storage system are presented in the following measurement campaign.

4.2. Charging Period: Electrical Heating

The charging of the storage system is based on heating wires, which are homogeneously distributed within the honeycombs heating the storage inventory via thermal radiation. For investigation of the transient heating process as well as the (optional) active cooling in the bypass path, variation studies on the heating power (1–6.8 kW) at a given charging duration (30 min) were conducted in this measurement campaign. The maximum permitted heating wire and bypass temperatures, which cause the activating of the active cooling when exceeded, were set to values of 1050 °C and 60 °C, respectively.

For an exemplary measurement at a heating power of 6.8 kW, the resulting transient characteristics in the bypass path and the inventory temperatures are shown in Figures 7 and 8.

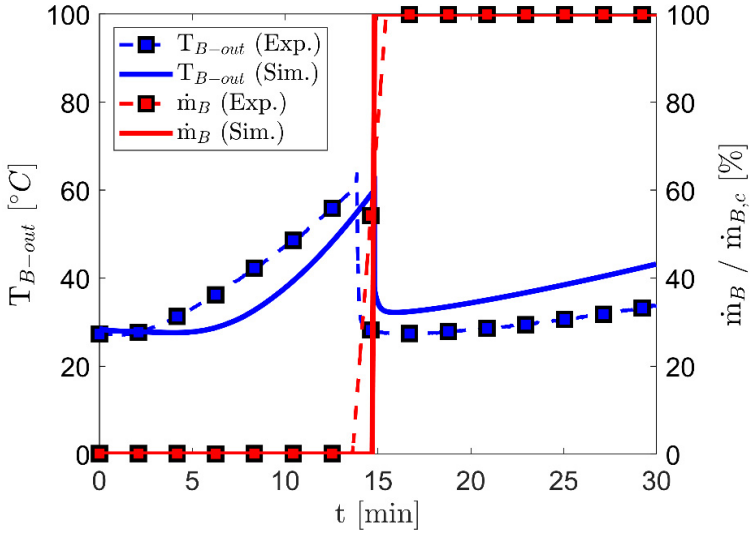

Figure 7. Transient characteristics in the bypass path: outlet temperature (T_{B-out}) and normalized active cooling mass flow rate ($\dot{m}_B/\dot{m}_{B,c}$).

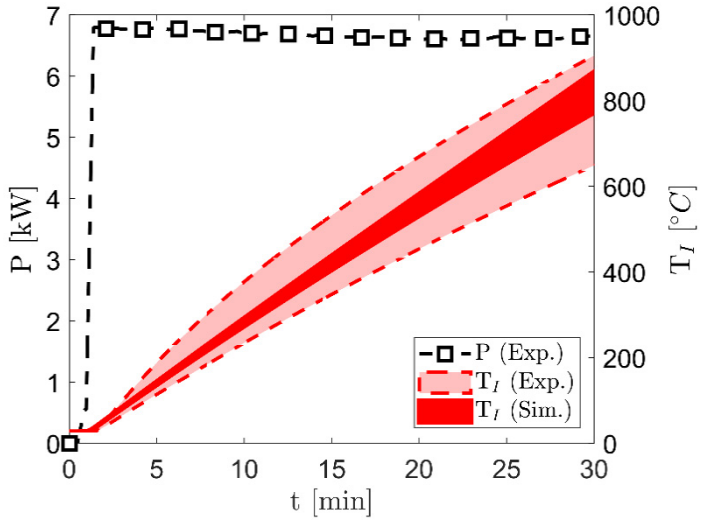

Figure 8. Transient temperatures in the honeycombs (T_I) and electric heating power (P).

The results during charging period of the storage system show increasing temperatures in the bypass path due to heat conduction and radiation coming from the heated honeycombs until the permitted maximum temperature of 60 °C is exceeded. From this point on, the active cooling is activated, whereby its magnitude is determined according to Equation (1). In comparison between the experimental and simulated results, a good agreement is evident both in characteristics of the bypass temperatures and in the time

for starting the active cooling. Due to the specified charging duration of only 30 min, the steady state condition of the bypass outlet temperature is not reached here.

Even in the temporal characteristics of the inventory temperatures, a good agreement between measurement and simulation is reached. After the beginning of electrical heating, the storage inventory temperatures increase until average values of 790 °C are reached in the measurement and 819 °C in the simulation at the end of charging period. The significantly higher spread in experimental results is due to the fact of only three radially distributed measurement locations (see Figure 4), whereby the outermost measuring zone was also integrated close to the shell-side thermal insulation. As a result, heat loss effects in combination with a limited number of thermocouples are disproportionately visible leading to elevated temperature spread inside the experimental results.

Comparable good agreements between the measurements and simulations—both in temporal characteristics of the temperatures and in times of activating the active cooling—were found in all investigations inside this measurement campaign. Central results on maximum inventory temperatures at the end of charging period as a function of heating power and on times of activating the active cooling are summarized in Figure 9 and in Table 3.

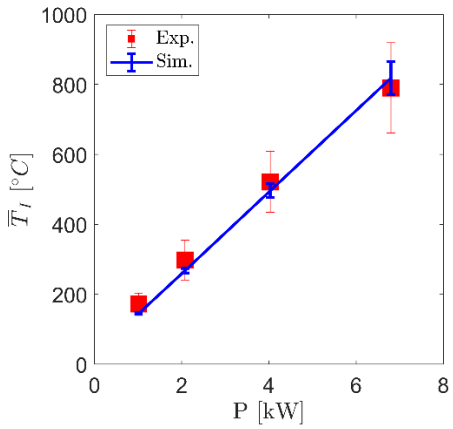

Figure 9. Average inventory temperatures ($\overline{T}_I$) at the end of charging period after 30 min.

Table 3. Time of activating the active cooling (t_c).

P [kW]	t_c [min] (Exp.)	t_c [min] (Sim.)
2	33.5 *	27.2
4	21.3	19.3
6.8	14.6	15.2

* Measuring period here slightly extended.

The results show—in good agreement between experiment and simulation—linear increasing inventory temperatures with raising constant heating powers. Relating to time of activating the active cooling summarized in Table 3 slightly lower values in the simulations compared to the measurements are visible. This is due to neglection of the double-walled containment mass in the model leading to a lower thermal capacity of the whole storage system. At low heating powers (1 kW) with the associated inventory temperatures of less than 200 °C, the permitted maximum bypass temperature of 60 °C was not exceeded, resulting in a non-activating of the active cooling in both the experimental und simulation results.

Based on the contexts explained here during charging period, investigations into the thermal discharging process of the storage system were conducted in the subsequent measurement campaign. The results presented in the following are only focused on discharging, whereby the charging procedure correspondents to the characteristics described in this section.

4.3. Discharging Period

During thermal discharging, cold entering air is passing the honeycombs and the bypass path via a mass flow control in order to achieve constant mixing temperatures at the outlet of the storage system. The fluid flow temperature is elevated convectively either from the previously electrical heated honeycombs or from the heat losses inside the bypath path. For investigation of the reachable discharging durations, variations studies were conducted regarding the constant mixing temperature (T_{out}), the total mass flow rate ($\dot{m}$) and the average inventory temperature ($\overline{T}_I$) at the end of charging period as summarized in Table 4.

Table 4. Central variation parameters: average inventory temperature ($\overline{T}_I$) at the end of charging period, total mass flow rate ($\dot{m}$), constant mixing temperature (T_{out}).

$\overline{T}_I$ [°C]	$\dot{m}$ [kg/h]	T_{out} [°C]
340	64	60
517	125	120
701	183	
843	230	

Here during charging period, the electrical heating's of the honeycombs were performed with a (constant) heating power of 6.8 kW up to the specified average inventory temperature for each measuring point. As in the previous section, the maximum permitted heating wire and bypass temperatures, which cause the activation of active cooling when exceeded, were set to values of 1050 °C and 60 °C, respectively. Central results regarding transient characteristics during discharging for an exemplary selected measurement at $\overline{T}_I$ = 843 °C and T_{out} = 120 °C each with $\dot{m}$ = 183 kg/h are shown in Figures 10–12.

With regard to the temporal and local temperatures inside the honeycomb, the results in Figure 10 illustrate the typical undulatory character of solid media thermal energy storage systems (regenerator): the entering cold air is convectively heated from the honeycomb over the flow path length leading locally to a cooling of the solid medium over time. Here, the efficiency of heat transport depends only on the heat transfer coefficient, the thermal resistance inside the solid medium and the heat transferring surface and is reflected in local and temporal temperature gradients. Within the scope of the honeycombs investigated here with their large specific surface areas of 620 m^2/m^3, high heat transfer rates are achieved, which are visible both in the experimental and comparably in the simulative results, respectively.

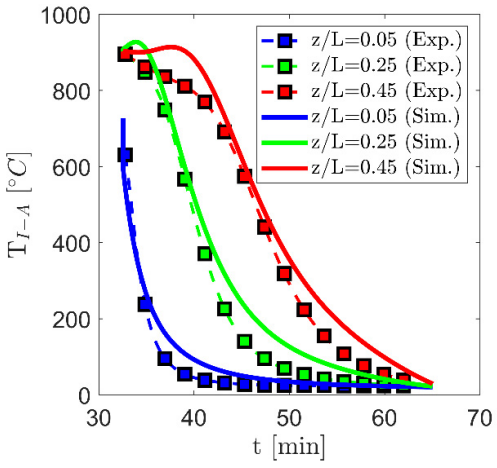

Figure 10. Transient temperature profiles in the honeycombs at z/L = 0.05 ($T_{I\text{-}A\text{-}1}$), 0.25 ($T_{I\text{-}A\text{-}2}$), 0.45 ($T_{I\text{-}A\text{-}3}$).

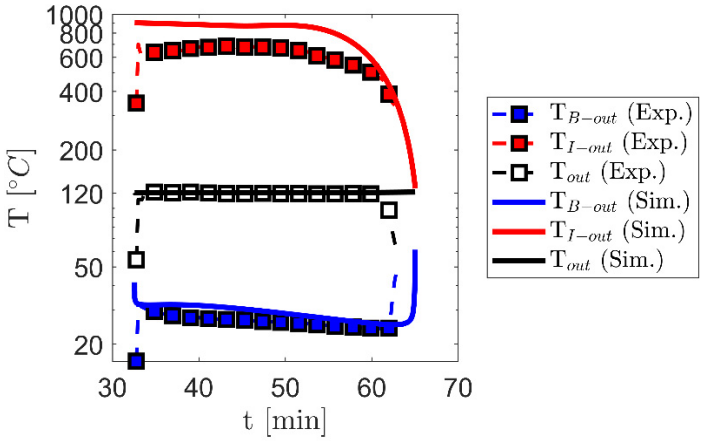

Figure 11. Transient temperature characteristics at the outlet of the storage inventory (T_{I-out}), the bypass path (T_{B-out}) and the storage system (T_{out}).

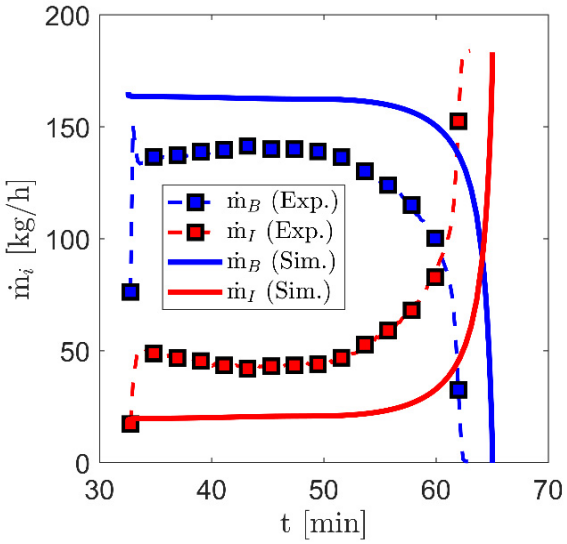

Figure 12. Transient characteristics of the mass flow rates inside the bypass path ($\dot{m}_B$) and storage inventory ($\dot{m}_I$).

In addition to the local characteristics within the honeycombs, the outlet temperatures of the storage inventory and the bypass path as well as the resulting constant mixing temperature are of central importance for the efficiency of the whole storage system. The results on this are shown in Figure 11.

As can be seen during discharging period, constant mixing temperatures of 120 °C are reached with a duration of 33 min in the simulation results and of approx. 29 min in the experimental results. Thereby over a long period of time, a relative constant level of temperatures at the outlet of the storage inventory and the bypass path are reached. At the solid medium side significant higher deviations between simulation and measurement are visible with average temperatures of approx. 870 °C and 650 °C, respectively. The main reasons for this are neglected heat losses at the front surfaces of the honeycombs inside the model. These lead locally to increased exergy losses of the exiting air, but only to slight energetic losses related to the stored thermal energy. Together with low requirements of the exiting constant air temperature compared to the storage inventory (see Figure 10), the described exergy losses effects only slightly the overall efficiency and thus the discharging duration.

However, in the last period of discharging significant temperature changes are visible in both flow paths. This effect is due to the specification of a constant mixing outlet

temperature—thus constant thermal discharge power—and related to the mass flow rates as shown in Figure 12.

Due to the specification of a constant mixing temperature, the mass flow rate in the bypass and inventory path shows an opposite behavior compared to the local outlet temperatures in time. Particularly in the last discharge period, high gradients are visible analogous to Figure 11. The reason for this is the interaction of increasing temperature drop of the air leaving the storage inventory with increasing mass flow rate. This positive feedback leads to growing gradients in the temporal mass flow rates and outlet temperatures and can be seen in good agreement in both the measurement and the simulation results.

Comparable to the characteristics explained here, good agreements between the experimental and simulative results with regard to constant mixing temperature, total mass flow rate and average inventory temperature at the end of charging period were found in all the investigations within this measurement campaign. For a comprehensive analysis and for evaluating the performance of the storage system, the thermal discharging power ($\dot{m}$) and the effective discharge duration (τ), which reflects the period of a constant mixing temperature (T_{out}), are suitable criteria. Here, the effective discharge duration is determined uniformly according to Equation (2) on the base of a maximum permitted deviation of the time dependent temperature difference ($T_{out}(\tau) - T_{in}$) to the specified temperature difference ($T_{out} - T_{in}$).

$$\left| 1 - \frac{T_{out}(\tau) - T_{in}}{T_{out} - T_{in}} \right| < 0.1 \tag{2}$$

The results for this as a function of the average inventory temperature at the end of charging period ($\overline{T}_I$) are summarized in Figure 13.

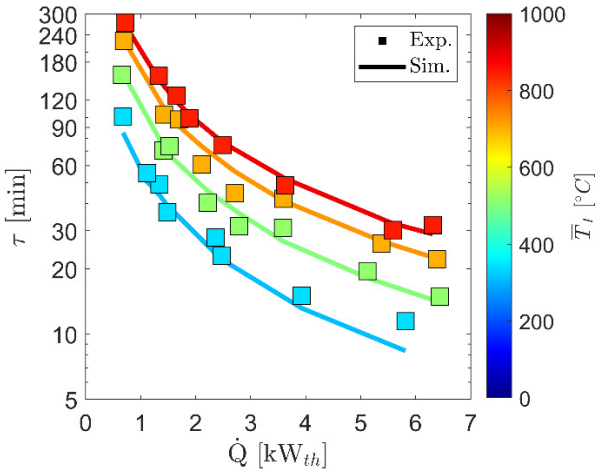

Figure 13. Effective discharge durations (τ) as a function of constant thermal discharge powers ($\dot{Q}$) and average inventory temperatures at the end of charging period ($\overline{T}_I$).

The investigations conducted show a direct correlation between these central quantities in both the simulative and the experimental results: increasing average inventory temperatures—thus thermal energy stored—as well as lower thermal discharge powers enable longer effective discharge durations. It is also obvious that the specified target values—constant thermal discharging with 5 kW over 30 min—were reached, whereby average inventory temperatures of approx. 700 °C are required for this. These temperatures can be achieved thereby with the currently available heating power of 6.8 kW in less than 30 min during charging period as illustrated in Figure 9.

Based on the findings obtained here, central results for evaluation of the systemic performance and optimization potentials of the storage system are presented in the following.

4.4. Overall Evaluation

The overall evaluation of the thermal storage system in terms of performance and optimization potentials is based on three key criteria: systemic storage density, effective heating power and parasitic losses.

Systemic storage density

The primary objective in the development of the novel thermal energy storage system for an alternative heat supply in battery electric vehicles is to achieve comparable or higher systemic storage densities in relation to today's battery-powered PTC heating elements. For this purpose, the results obtained in the previous section regarding effective discharge duration and constant thermal discharge power are considered in relation to the total mass of the storage system. The resulting systemic storage densities from this—thus the effectively usable heat at a constant temperature or thermal power level—are illustrated in Figure 14.

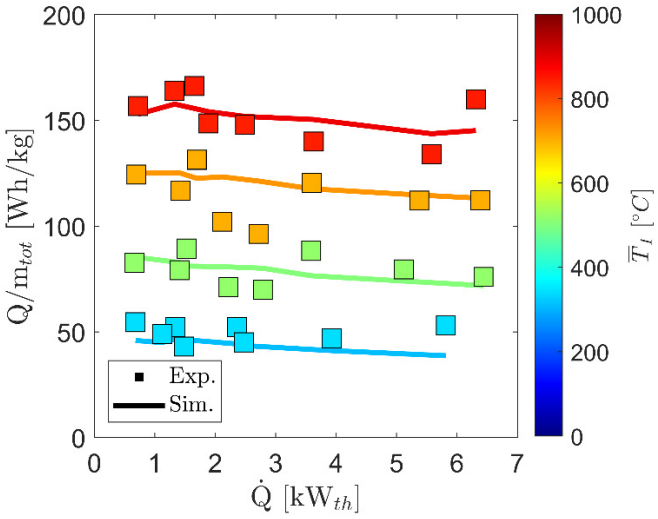

Figure 14. Systemic storage density (Q/m_{tot}) as a function of constant thermal discharge powers ($\dot{Q}$) and average inventory temperatures at the end of charging period ($\overline{T}_I$).

The results show a constant level of systemic storage densities within the considered thermal discharge power range of up to 6.4 kW, whereas their magnitudes depend on the average inventory temperatures at the end of charging period. Minor decreases in systemic storage density with increasing constant thermal discharge power are visible, associated with the higher requirements for heat transport of the air passing the honeycombs. For the maximum average inventory temperatures currently achieved at the end of charging period of approx. 843 °C, systemic storage densities of approx. 155 Wh/kg are reached in the experimental and in the simulative results. Compared to today's PTC heaters with battery-specific storage densities of up to 160 Wh/kg [25], the performance of the first thermal storage system test rig is already visible. Further increases of the systemic storage density up to 200 Wh/kg can be achieved by optimizations, regarding the inventory material and its void fraction, by layered thermal insulation concepts and reduced heating wire lengths as well as design improvements on the double-walled containment.

Effective heating power

In addition to the high performance achieved by the thermal storage system during discharging period, the results presented in Section 4.2 also show high effective heating powers during charging. Thus, with maximum permitted heating wire temperatures of 1050 °C, a constant heating power of 6.8 kW could be achieved up to average inventory temperatures of approx. 843 °C. From this level, the implemented control leads to a reduction of the heating power, whereas currently a further increase of the average inventory temperatures up to 880 °C was reached. Additional improvements in performance during charging period can be obtained by a more homogeneous distribution of the heating wires

within the honeycombs and by higher permitted heating wire temperatures up to the operational limit of 1300 °C. Apart from that, the electrical connection of the three heating wires limits the maximum heating power to approx. 6.8 kW due to the current laboratory restrictions. Despite these limitations, the heat of 2.5 kWh required for thermal discharge could be generated and stored in less than 30 min during the charging period fulfilling successfully the target values specified for the investigated test rig. By futural adapting the laboratory infrastructure on a 32 A system and a delta circuit of the heating wires, heating powers of up to 19.2 kW can be reached allowing significant improvements in charging durations on less than 11 min.

Parasitic losses

The central issue for optimization includes the balance between permitted heat losses and the amount of thermal energy used for preheating the interior via the double-walled bypass path during charging period, respectively. For the current test rig under investigation, heat losses inside the active cooling flow rate with maximum magnitudes of approx. 500 W were measured. Although this waste heat can be directly used for preheating through the implemented mass flow control, there is still a need for optimization in terms of a holistically balanced thermal storage system and operating concept. With low adaptions regarding layered thermal insulations at the shell-side and improved thermal insulations at the front faces, considerable reductions in heat losses can be reached without losing systemic storage densities significantly.

In addition, pressure losses arise inside the storage systems and must be considered carefully while designing promising geometrical solutions. However, inside the experimental investigations presented here pressure losses were not measured but are calculated in advance within the simulation studies performed in [24,26]. Maximum values of less than 5 mbar for both paths were identified here due to high void fractions inside the selected honeycombs and a relatively high duct width inside the double-walled bypass path. However, additional flow resistances are to be expected within the internal distributors and the mixing zone requiring CFD based simulations together with overall volume-specific optimizations.

4.5. Operational Flexibility

The results explained so far focused on cyclic storage operation with the associated findings regarding systemic storage density, constant discharge and effective heating power. However, regardless of the optimization potentials still to be achieved, every storage system requires subsequent charging after complete discharging in order to maintain its functionality and thus its use.

For the component developed here, an improved flexibility is given due to its integrated electric heating system allowing a bifunctional operational use: on the one hand as storage system with successive charging/discharging periods and on the other hand as convective heating system. For using the component in the heating mode, the air to be heated is passed through the honeycombs only, while the electric heating system is activated at the same time. First results for this operating mode with a heating power of 2.5 kW and inlet temperatures of 20 °C are shown in Figure 15.

The characteristics show a decrease in the outlet temperatures with increasing mass flow rates with a good agreement between the experimental and simulative results. Compared to conventional PTC heaters, however, the significantly larger component mass within the system leads to increased thermal inertia resulting in lower dynamics when reaching steady state conditions. Despite this, it is obvious that the component developed here allows variable heating operations in addition to the cyclic storage mode. Due to its flexibility, the operating time and thus the utilization of the component can be improved significantly without increasing the overall systemic complexity inside the battery electric vehicle.

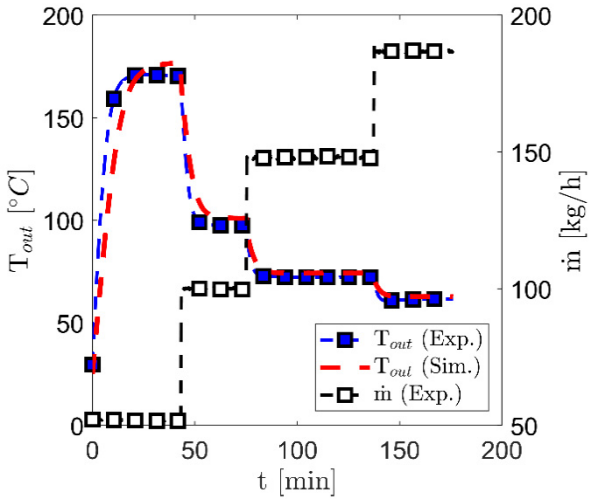

Figure 15. Heating mode—transient outlet temperature (T_{out}) as a function of the air mass flow rate ($\dot{m}$).

5. Conclusions

A key element for improving efficiency and flexibility are thermal energy storage systems. They store efficiently heat available or generated in processes at times of low thermal energy demand (charging period) and provide it at times of increased thermal energy demand (discharging period). Such solutions, extended by power-to-heat options, are already commercially available in large-scale applications or are in focus in a wide range of R&D activities, but new in the transport sector. By transferring existing ideas as new thermal management concepts for battery electric vehicles an alternative heat supply during cold seasons can be enabled reducing the battery-powered heating demand and thus increase the effective range.

In particular, through vehicle-specific weight restrictions solutions are needed that achieve high systemic storage and power densities while at the same time meeting thermal requirements in terms of performance and temperature level. For this purpose and for the first time, a novel thermal storage system based on an electrically heated solid medium has been developed, constructively realized, systematically measured and successfully validated. High-temperature heat is generated electrically in heating wires during the charging period and transferred efficiently via thermal radiation to ceramic honeycombs. During discharging period, the stored thermal energy is used to heat the interior at defined temperature levels with high thermal powers by a bypass control.

Despite test rig-related limitations, the experimental results confirm the feasibility of meeting all vehicle-specific requirements and simultaneously achieving high systemic storage and power densities. Under the existing laboratory infrastructure, the thermal energy storage system reaches constant heating powers of 6.8 kW up to average inventory temperatures of approx. 843 °C. During discharging period constant thermal powers of up to 6.4 kW at adjustable temperature levels are reached leading to systemic storage densities of about 155 kWh/kg. In addition, the developed component also allows high flexibility through a bifunctional operational use: on the one hand as storage system with successive charging/discharging periods and on the other hand as convective heating system.

Future activities will focus on the implementation of improvement measures based on the identified optimization potentials regarding inventory materials, thermal insulations, electric heating wires and double-walled storage containment. With a successful implementation, systemic storage densities of up to 200 Wh/kg and maximum heating powers of up to 19.2 kW will be expected. In addition to a prototypical realization with reduced amount of measurement devices and thus significantly high volume-specific improvements, conceptual investigations on system extensions for generation and storage of cold are performed. Here, basic idea is to increase the seasonal utilization of the novel

component by using it in hot seasons as source for cold supply and thus to achieve further efficiency improvements for battery electric vehicles.

Author Contributions: Conceptualization, L.H.; investigation, V.D.; methodology, V.D.; validation, V.D. and L.H.; writing—original draft, V.D. All authors have read and agreed to the published version of the manuscript.

Funding: This research received no external funding.

Conflicts of Interest: The authors declare no conflict of interest.

References

1. Kuper, C.; Hoh, M.; Houchin, G.-M.; Fuhr, J. *Thermal Management of Hybrid Vehicle Battery Systems*; EVS24: Stavanger, Norway, 2009.
2. Jung, M.; Kemle, A.; Strauss, T.; Wawzyniak, M. *Innenraumheizung von Hybrid—Und Elektrofahrzeugen*; ATZ: Vancouver, BC, Canada, 2011; pp. 396–401.
3. Pradeep, N.; Reddy, K.S. Design and investigation of solar cogeneration system with packed bed thermal energy storage for ceramic industry. *Renew. Energy* **2022**, *192*, 243–263. [CrossRef]
4. Amelio, M.; Morrone, P. Numerical evaluation of the energetic performances of structured and random packed beds in regenerative thermal oxidizers. *Appl. Therm. Eng.* **2007**, *27*, 762–770. [CrossRef]
5. Krüger, M.; Muslubas, S.; Loeper, T.; Klasing, F.; Knödler, P.; Mielke, C. Potentials of Thermal Energy Storage Integrated into Steam Power Plants. *Energies* **2020**, *13*, 2226. [CrossRef]
6. Alami, K.E.; Asbik, M.; Agalit, H. Identification of natural rocks as storage materials in thermal energy storage (TES) system of concentrated solar power (CSP) plants—A review. *Sol. Energy Mater. Sol. Cells* **2020**, *217*, 110599. [CrossRef]
7. Dreißigacker, V.; Belik, S. System configurations and operational concepts for high efficient utilization of Power-to-Heat in A-CAES. *Appl. Sci.* **2019**, *9*, 1317.
8. Steinmann, W.-D.; Bauer, D.; Jockenhöfer, H.; Johnson, M. Pumped thermal energy storage (PTES) as smart sector-coupling technology for heat and electricity. *Energy* **2019**, *183*, 185–190. [CrossRef]
9. Marongiu, F.; Soprani, S.; Engelbrecht, K. Modeling of high temperature thermal energy storage in rock beds—Experimental comparison and parametric study. *Appl. Therm. Eng.* **2019**, *163*, 114355. [CrossRef]
10. Yin, H.; Ding, J.; Jiang, R.; Yang, X. Thermocline characteristics of molten-salt thermal energy storage in porous packed-bed tank. *Appl. Therm. Eng.* **2017**, *110*, 855–863. [CrossRef]
11. Wang, F.; Zheng, W.; Gou, Y.; Jia, Y.; Li, H. Thermal behaviors of energy storage process of eutectic hydrated salt phase change materials modified by Nano-TiO_2. *J. Energy Storage* **2022**, *53*, 105077. [CrossRef]
12. Salgado-Pizarro, R.; Calderón, A.; Svobodova-Sedlackova, A.; Fernández, A.I.; Barreneche, C. The relevance of thermochemical energy storage in the last two decades: The analysis of research evolution. *J. Energy Storage* **2022**, *51*, 104377. [CrossRef]
13. Belik, S.; Dreissigacker, V.; Zunft, S. Power-to-heat integration in regenerator storage: Enhancing thermal storage capacity and performance. *J. Energy Storage* **2022**, *50*, 104570. [CrossRef]
14. Korin, E.; Reshef, R.; Tshernichovesky, D.; Sher, E. *Improving Cold-Start Functioning of Catalytic Converters by Using Phase-Change Materials*; SAE Technical Papers Ser.; SAE: Warrendale, PA, USA, 1998. [CrossRef]
15. Gumus, M. Reducing cold-start emission from internal combustion engines by means of thermal energy storage system. *Appl. Therm. Eng.* **2009**, *29*, 652–660. [CrossRef]
16. Engel, G. Sorption cold storage for thermal management of the battery of a hybrid vehicle. *Energy Procedia* **2018**, *155*, 149–155. [CrossRef]
17. Dieterich, M.; Bürger, I.; Linder, M. Open and closed metal hydride system for high thermal power applications: Preheating vehicle components. *Int. J. Hydrogen Energy* **2017**, *42*, 11469–11481. [CrossRef]
18. Kölbig, M.; Bürger, I.; Schmidt, M.; Linder, M. Thermal applications in vehicles using Hydralloy C5 in single and coupled metal hydride systems. *Appl. Energy* **2021**, *287*, 116534. [CrossRef]
19. Ugurlu, A.; Gokcol, C. A review on thermal energy storage systems with phase change materials in vehicles. *Electron. J. Vocat. Coll.* **2012**, *2*, 1–14.
20. Kraft, W.; Stahl, V.; Vetter, P. Thermal Storage Using Metallic Phase Change Materials for Bus—State of the Art of Electric Buses and Requirements for the Storage System. *Energies* **2020**, *13*, 3023. [CrossRef]
21. Xie, P.; Jin, L.; Qiao, G.; Lin, C.; Barreneche, C.; Ding, Y. Thermal energy storage for electric vehicles at low temperatures: Concepts, systems, devices and materials. *Renew. Sustain. Energy Rev.* **2022**, *160*, 112263. [CrossRef]
22. Javani, N.; Dincer, I.; Naterer, G.F. New latent heat storage system with nanoparticles for thermal management of electric vehicles. *J. Power Source* **2014**, *268*, 718–727. [CrossRef]
23. Sergej, B.; Dreißigacker, V.; Dieterich, M.; Kraft, W. Next Generation Car Thermal energy storage systems: Power-to-Heat concept in solid media storage for high storage densities. In Proceedings of the EVS30 Symposium, Stuttgart, Germany, 9–11 October 2017.
24. Dreißigacker, V. Solid Media Thermal Energy Storage System for Heating Electric Vehicles: Advanced Concept for Highest Thermal Storage Densities. *Appl. Sci.* **2020**, *10*, 8027. [CrossRef]

25. Hannan, M.A.; Hoque, M.M.; Hussain, A.; Yusof, Y.; Ker, P.J. State-of-the-Art and Energy Management System of Lithium-Ion Batteries in Electric Vehicle Applications: Issues and Recommendations. *IEEE Access* **2018**, *6*, 19362–19378. [CrossRef]
26. Dreißigacker, V. Thermal Battery for Electric Vehicles: High-Temperature Heating System for Solid Media Based Thermal Energy Storages. *Appl. Sci.* **2021**, *11*, 10500. [CrossRef]
27. Wang, M.; Wolfe, E.; Craig, T.; Laclair, T.; Abdelaziz, O.; Gao, Z. *Design and Testing of a Thermal Storage System for Electric Vehicle Cabin Heating*; SAE Technical Paper 2016-01-0248; SAE: Warrendale, PA, USA, 2016. [CrossRef]
28. Luo, C.; Xie, P.; Chen, G.; Mao, L.; Liu, L.; Jin, L.; Cheng, Z.; Xu, J.; Qiao, G. Prototype design and experimental study of a metal alloy-based thermal energy storage system for heat supply in electric vehicles. *J. Energy Storage* **2022**, *51*, 104393. [CrossRef]